Induction Thermography of Surface Defects

41

Udo Netzelmann

Contents

U. Netzelmann (✉)

Fraunhofer-Institute for Nondestructive Testing IZFP, Saarbrücken, Germany
e-mail: udo.netzelmann@izfp.fraunhofer.de

Abstract

A survey on theory, characteristic quantities, and the experimental technique of induction thermography is given. Induction thermography is used for surface defect detection in forged parts of ferromagnetic steel at typical frequencies of 100–300 kHz. Values for the detection limits for various types of cracks and approaches to determine crack depths are given. The sensitivity for crack detection is comparable to magnetic particle inspection. A hidden defect in ferritic steel with a coverage of 140 µm was detected by lowering the induction frequency down to 1500 Hz. Cracks in silicon solar cells were detected. Defects of fibers were detected in carbon fiber-reinforced polymer (CFRP). Inductive excitation is complementary to flash excitation. Crack detection in railway components like rails and wheels is shown. In rails, a larger defect could be detected from a test car moving at a speed of up to 15 km/h. A fully automated demonstrator for wheel testing was built up, which can detect surface defects in railway wheels with sensitivity comparable to magnetic particle testing. Standardization of thermography has gained progress in the last years and led to first standards on active thermography and induction thermography.

Introduction to Induction Thermography

Induction thermography or pulsed eddy current thermography uses electromagnetic pulses to excite eddy currents in electrically conductive materials. An inductor (Fig. 1) is positioned at a certain distance from a surface to be tested for surface defects like cracks. In the test object, eddy currents i_{ec} are induced that form closed loops in the material. The currents have to circumvent the cracks. This causes local changes of the electrical current densities in the material. The eddy currents generate heat by resistive losses. The heat can be detected by an infrared camera observing the surface. Around cracks, the current density is changed, e.g., increased at the crack tips. As heat generation is proportional to the square of the current density, the cracks will form a characteristic thermal pattern on the surface which has a specific time dependence that reveals the position and the orientation of the crack.

First applications in the steel industry were reported more than three decades ago (Kremer 1984). The Therm-O-Matic system was applied to detect longitudinal cracks by continuous inductive heating of moving steel bars. The speed relative to the coil was up to 1 m/s. Several of these systems are still in operation today. Further, the technique has been applied using periodic heating and phase sensitive detection for characterization of the adhesion of rubber on aluminum (Heath and Winfree 1990). A ferrite core transducer was used for excitation. Pulsed high-frequency burst excitation is used in the production process for detection of cracks in turbine blades (Bamberg et al. 1999). These tests are part of the internal component qualification by the manufacturer. Further applications were reported on compressor blades and tensile test specimens, as well as on impact damage detection in carbon fiber reinforced polymers (Riegert et al. 2004). There was significant work on analytical

Fig. 1 Scheme of induction thermography
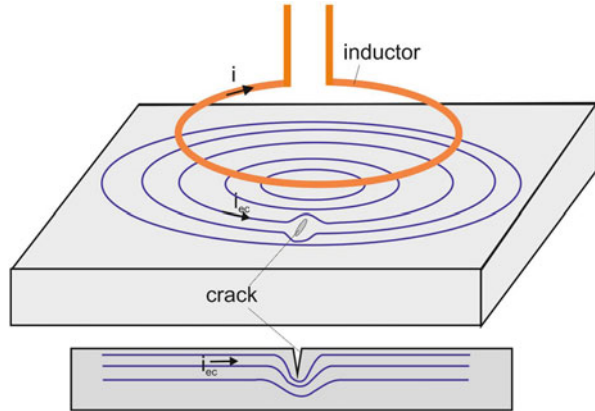
and numerical modelling of the signal from cracks in steel (Oswald-Tranta 2004). The current distribution and the resulting heating were calculated, providing insight into the contrast formation. The signal contrast was analyzed experimentally as a function of crack length, crack depth, and crack orientation (Walle and Netzelmann 2006). In Vrana et al. (2008), the current flow in small components was studied including the proximity effect. The contrast from cracks filled with conducting materials was investigated. Recent applications were devoted to testing of adhesive bonds of aluminum sheets for automotive application (Balaji et al. 2013) and describe carbon fiber laminate testing (He et al. 2014).

In this contribution, first, the characteristic electric and thermal quantities will be discussed. After a description of the experimental setup, detection of various types of cracks will be described. Then examples will be shown for different application fields of induction thermography. A final remark is given to the present efforts for standardization.

Electromagnetic and Thermal Key Parameters

In contrast to eddy current testing, induction thermography has both an electromagnetic and a thermal aspect (Netzelmann and Walle 2008). In order to estimate the ability to detect defects in materials by induction thermography, one has to consider the electromagnetic skin depth δ, which describes the depth of the induction current flow. For a thick plane body, the electric and magnetic fields and the resulting currents are exponentially damped with the skin depth as a characteristic length, when propagating into the depth. It is given by

$$\delta = \sqrt{\frac{1}{\pi f \sigma_e \mu}}, \tag{1}$$

where σ_e is the electrical conductivity, μ the magnetic permeability, and f is the electromagnetic frequency. Another characteristic length is the thermal penetration depth μ_T. The depth of the thermal propagation for a given observation time t (in a pulsed experiment) is given by

$$\mu_T(t) = 2\sqrt{\alpha t} \tag{2}$$

Here, α is the thermal diffusivity of the material. In Fig. 2, the distribution of the induction currents, the heat sources, and the resulting thermal flow are sketched.

Examples for skin depth and thermal penetration depth for different materials for an induction frequency of $f = 100$ kHz and an observation time $t = 100$ ms are given in Table 1.

Thermal Response to Inductive Heating in Various Materials

Basic requirement for application of induction thermography is that there is an electrically conducting material. When a plane electromagnetic wave enters a conducting half-space, its field components and the induction currents are damped with the skin depth δ as characteristic length. The heat sources due to ohmic losses are proportional to the square of the induced currents. Therefore, the heat source
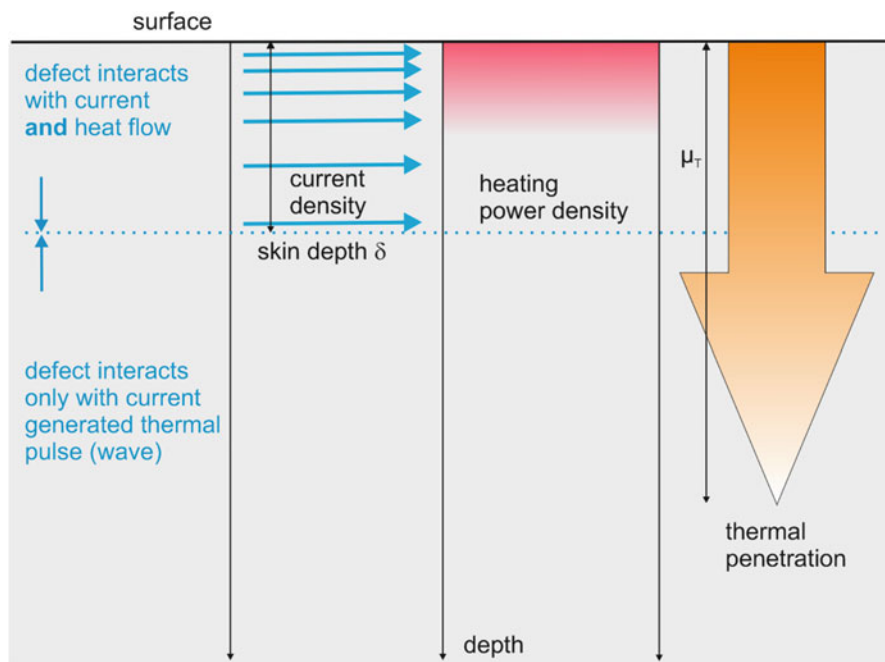

Fig. 2 Scheme of inductive heating and thermal propagation in a conducting material

Table 1 Material parameters, characteristic lengths and induction heating efficiency

Material group		Electrical conductivity in 10⁶S/m	Relative magnetic permeability	Thermal conductivity in W/(mK)	Electro-magnetic skin depth in mm (100 kHz)	Thermal penetration depth in mm ($t = 0.1$ s)	Surface temperature rise in K after 0.1 s heating with 0.02 T induction field amplitude at 100 kHz
I	**Cast iron**	6.2	200	49	0.045	2.43	12.4
	Nickel, pure	14.62	100	90.7	0.042	3.03	3.9
II	**Silver, pure**	62.87	1	408	0.201	8.15	0.1
	Zinc, rolled	16.24	1	113	0.395	4.06	0.4
	Aluminium 2014-T6	22.53	1	177	0.335	5.97	0.3
	Copper, pure	60.09	1	401	0.205	6.83	0.1
III	**Inconel 600**	0.98	1	14.9	1.608	1.26	1.6
	Stainless steel 316	1.33	1	13.4	1.380	1.18	1.5
	Titanium 6AL–4 V	0.58	1	7.2	2.090	1.08	2.9
IV	**Carbon fibre reinforced polymer perp. To fiber**	0.0001	1	0.7	159	0.39	5.3
	SiC ceramic	0.00005	1	80	225	3.36	3.5
	Silicon	0.001	1	148	50	6.11	5.8

distribution decays with a damping constant of $\delta/2$ into the depth z of the material. The heat source $q(z)$ can be described by

$$q(z) = \frac{b^2}{2\mu_0^2}\mu_0\mu_R 2\pi f \exp\left(-\frac{2}{\delta}z\right). \tag{3}$$

Here, b is the high-frequency magnetic field at the sample surface, μ_0 the permeability constant, and μ_R the high-frequency magnetic permeability ($\mu_R = (\mu_r'^2 + \mu_r''^2)^{0.5}$-$\mu_r''$, where μ_r' and μ_r'' are the real and the imaginary part of the complex relative permeability, respectively). At typical induction frequencies, μ_R is usually somewhat smaller than the static relative permeability (Bowler 2006).

When induction heating starts at the time $t = 0$, the resulting surface temperature change ΔT at the surface can be calculated based on a result in Carslaw and Jaeger (1959):

$$\Delta T = \frac{b^2}{2\mu_0^2}\mu_0\mu_R \frac{2\pi f}{\lambda}\delta^2\left(\frac{1}{2\sqrt{\pi}}\frac{\mu_T}{\delta} - \frac{1}{4}\left(1 - \exp\left(\left(\frac{\mu_T}{\delta}\right)^2\right)erfc\left(\frac{\mu_T}{\delta}\right)\right)\right). \tag{4}$$

Here, λ is the thermal conductivity of the material. The time dependence of ΔT is implicitly given by μ_T (Eq. 2). The temperature change is governed by the ratio of thermal penetration depth and electromagnetic skin depth. Equation 4 can be used to compare the thermal response of a material after a certain heating time caused by a given induction field at its surface (in the following called "induction heating efficiency"). Table 1 shows examples for material parameters and penetration depths and identifies several material groups in induction thermography. In its right column, Table 1 lists the surface temperature rise ΔT resulting from an induction field of $b = 0.02$ T at an induction frequency of $f = 100$ kHz after 0.1 s of inductive heating.

Four groups of materials can be identified in Table 1. Due to their high magnetic permeability, the ferromagnetic metals (group I) even after a short time have a very small skin depth compared to the thermal penetration. Only a thin surface layer generates the heat. The nonmagnetic metals in group II are often good electrical conductors, but their relative permeability is close to one. Their skin depth is still one order below the typical thermal penetration. In group III there are metallic alloys with relatively poor electrical and thermal conduction. Here, the electromagnetic and thermal penetration depth is of comparable size for the given parameters. Finally, the materials of group IV have an electromagnetic skin depth significantly larger than the thermal penetration.

The right column in Table 1 shows that the ferromagnetic metals form group I have the highest induction heating efficiency. On the other hand, the induction heating efficiency in group II is poor. In particular the aluminum alloys have efficiency about a factor of 30 below that of magnetic steel, rendering testing of these materials difficult. This is further complicated by their often low infrared emissivity. In spite of this, successful applications on aluminum were reported (Tsopelas and Siakavellas 2011).

For the materials in groups I and II after a very short time the thermal penetration is larger than the skin depth, $(\mu_T >> \delta)$. Then, Eq. 4 can be simplified to

$$\Delta T(t) = \frac{b^2}{2\mu_0^2} \mu_0 \mu_R 2\sqrt{\pi} f \delta \frac{\sqrt{t}}{\sqrt{(\lambda \rho c)}}. \tag{5}$$

Here, ρ and c are the density and the specific heat of the material, respectively. Experimentally, the surface heating process is characterized by a temperature rise proportional to the square root of time. As the skin depth δ is proportional to $f^{-0.5}$, the temperature rise ΔT is in total proportion to the square root of the induction frequency.

Due to their larger skin depth, the alloys from group III represent a transition from surface heating to volume heating. The induction heating efficiency is much better than that of group II. Indeed, many successful applications of crack detection in aeronautical or power generation turbine components with materials from group III were reported (Zenzinger et al. 2007).

Finally, the materials in group IV are characterized by $\mu_T << \delta$, even for longer times t. In this case, Eq. 4 can be simplified to

$$\Delta T(t) = \frac{b^2}{2\mu_0^2} \mu_0 \mu_R 2\pi f \frac{t}{\rho c}. \tag{6}$$

The surface temperature rises proportional to time, which is typical for a volume heat source. It is proportional also to the induction frequency. The induction heating efficiency does not reach that of magnetic steel but is better than that of the materials in group III. Successful applications, e.g., in carbon fiber-reinforced polymers, were reported (Liang et al. 2016; Guo et al. 2017).

The total power density S in W/m^2 absorbed by the sample can be obtained by integration of Eq. 3 over the depth z. It is given by

$$S = \frac{b^2}{2\mu_0^2} \sqrt{\frac{\pi \mu_0 \mu_R f}{\sigma_e}} \tag{7}$$

In all cases, higher magnetic permeability increases the signal, which explains the good induction efficiency in ferritic steel. For magnetic materials, Eqs. 3, 4, 5, 6, 7 are an approximation for small deviations of the magnetization from its equilibrium. It has been shown that static magnetic fields applied in addition to the high-frequency field can improve the thermographic contrast of cracks, when applied in a proper direction (Jäckel and Netzelmann 2013).

It should be mentioned that the electromagnetic skin depth as defined in Eq. 1 is valid for a plane electromagnetic wave incident to a plane, thick conductor. The dampling lengths will be somewhat different for rod and tube geometries, for thin plates, small components, and under inductor wires. Even more complicated are the current paths in anisotropic conductors like CFRP.

Instrumentation

A typical experimental setup with a pulsed excitation system is shown in Fig. 3. A high frequency induction coil in the neighborhood of the test object generates eddy currents in burst pulses of typically 50–500 ms length. The induction coil and capacitive elements in the workhead form a resonant circuit with large rf currents close to resonance. Pulsed excitation is the fastest way for testing of components, in particular, when mass products have to be inspected in the industrial environment. It should be noted that the resonant circuit consisting of workhead and coil needs some minimum settling time between zero and full induction power and vice versa. This may limit detection of smallest defects. The burst pulse length should be short enough not to miss the smallest defects but long enough to generate sufficient defect contrast.

Alternatively, excitation can be generated by nonresonant high power amplifiers (preferably in the frequency range < 50 kHz). A fast rise-time of the induction current is possible.

Another possibility, in particular when the available maximum induction power is low, is amplitude modulation of the high-frequency signal at a lower modulation frequency f_{mod}. A gateable frequency generator can be used, followed by a broad-band power amplifier. Then, a lock-in algorithm is applied to the recorded time-depended signal of each pixel in order to calculate amplitude and a phase image (Riegert et al. 2004). Periodic excitation is used mainly in the laboratory or at induction frequencies, where high-power pulses are hardly available. Compared to
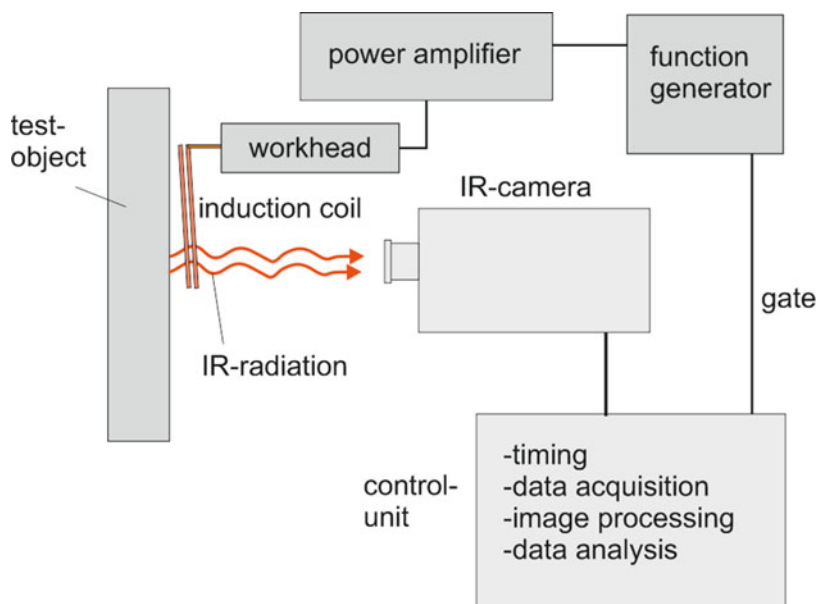

Fig. 3 Scheme of a set-up for induction thermography

pulsed operation, the measurement time to achieve a given signal/noise ratio will be generally longer.

Camera, induction coil, and test object can also be in relative movement. Then, the induction coil is operated in a cw mode. For testing of long tubes and steel bars, encircling coils are used. A time dependent excitation is caused by the relative movement (see a later section).

A less common possibility to generate time-dependent heat flows is to move a permanent magnet with sufficient relative speed to the test object. This will induce eddy currents that generate heat (principle of the eddy-current brake) (Netzelmann 2006).

Inductors

The induction coils used can be similar to those used for induction hardening or other industrial heating tasks (Fig. 4). They can be air coils with or without water cooling. Water cooling will be necessary for continuous operation of the coil, e.g., for relative movement between test object and coil, or for fast testing cycles. Helmholtz coils were reported that have the advantage to homogenize the excitation field and to allow full optical access to the component surface for the infrared camera
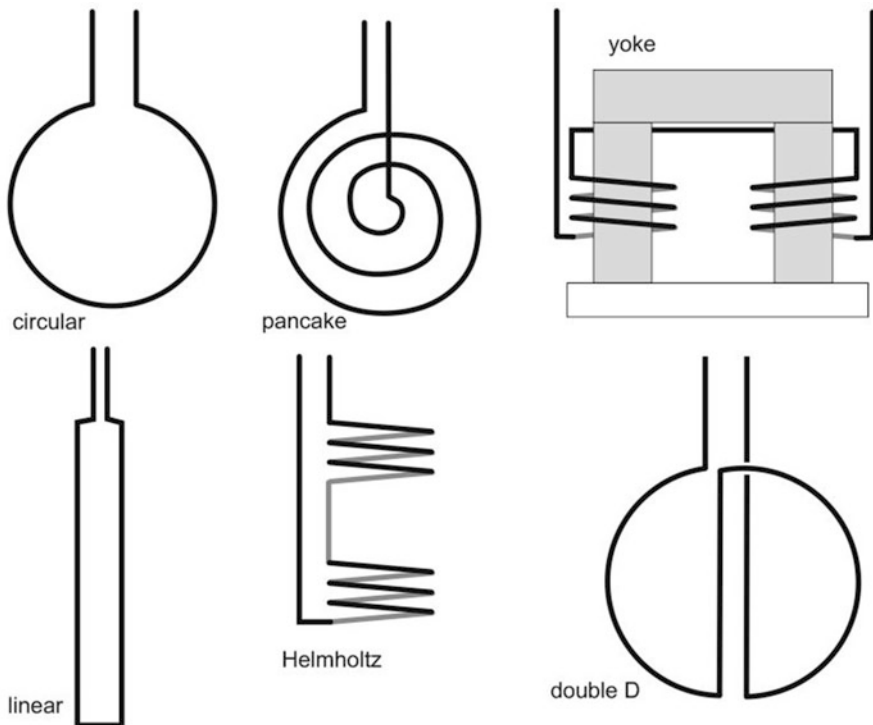

Fig. 4 Typical inductors as used for induction thermography

(Wilson et al. 2010). The magnetic flux of a coil can be concentrated by using a yoke made out of a material with high permeability. Linear coils can be used for inspection objects on a moving conveyor belt. Double D coils homogenize the magnetic field in the area between the parallel wires. Other inductor concepts use two orthogonally oriented yokes that are fed by currents which are 90° phase shifted in order to form a rotating induction field (Tang et al. 2018). Using this, the crack signal is less sensitive to the crack orientation versus the induction current.

Covering the winding of the coil by a thermally thick insulator helps reduce time-dependent thermal radiation from resistive losses in the coil.

Infrared Cameras

The infrared camera is used to record image sequences of the surface radiation from shortly before until sometime after the heating pulse (Fig. 3). Two types of detectors are common:

The bolometer detector is a thermal detector for infrared radiation and allows frame-rates up to about 60 Hz. They are typically sensitive in the 7–15 μm wavelength range. These detectors have seen significant technical progress with respect to sensitivity and pixel resolution. Models with 1920×1080 pixels resolution have become available. The noise equivalent temperature deviation (NETD) may go down to 30 mK or less. Thermal detectors represent the most cost-efficient and a low-maintenance solution. They are sufficient to solve a large class of testing applications.

Infrared cameras based on photon detectors are more sensitive (NETD down to 10 mK), show less or no crosstalk between neighboring pixels, and offer short integration times and high frame-rates. They are typically sensitive in the 2–5.5 μm wavelength range (mid-wave infrared, MWIR) but also available for the longer wavelengths. A cooling system is required. The resolution currently goes up to 640×512 pixels or higher. For detection of smallest defects, this camera type is the best choice. The price is significantly higher than that of a bolometer camera and the detector coolers have limited lifetime.

Both camera types need a possibility for synchronization of the image acquisition (at least by a frame time-stamp) with the excitation. Bolometer cameras must allow the deactivation of the built-in shutter for drift- and nonuniformity correction during the time of image acquisition.

For induction thermography, photon detector cameras will be preferably used for testing materials with high thermal conductivity and low induction efficiency, whereas bolometer cameras may be sufficient for materials with high induction efficiency or for poor conductors like CFRP.

Pre-Processing of the Recorded Image Sequences

A pre-processing of the recorded image sequences has as a major task to suppress the local inhomogeneity of inductive heating and to extract time-dependent signals that

are characteristic for many defects. A frequently used technique applied in the case of excitation by high-frequency bursts is the pulse-phase transform (PPT). The time dependent signal from each pixel in the image is transformed into the frequency space. From the results, amplitude and phase images in the frequency space are generated. A common practice is to transform a time interval of $t_p + t_c$, where t_p is the length of the burst pulse and t_c a cooling time after the pulse. Amplitude and phase images at the frequency of $1/(t_p + t_c)$ and its multiples will result. The phase images will largely be free of the inhomogeneous distribution of induction currents (which is almost unavoidable in induction thermography) or of local variations of surface emissivity. Characteristic phase shifts around cracks will appear more clearly with better signal/noise ratio. Varieties of other pre-processing techniques like principal component analysis are available and have been investigated.

In the case of periodic modulation, conventional processing of the recorded image sequences by lock-in algorithms is performed.

Defect Detection

Detectable Types of Defects

In a previous chapter, it has been pointed out that the interaction with defects in induction thermography is based on electromagnetic and thermal interaction with the defect (Fig. 2). These interactions determine the detectability of defects. In Fig. 5, typical defects are shown in a cross-section through an electrically conducting material. The skin depth δ is indicated as a zone at the surface.
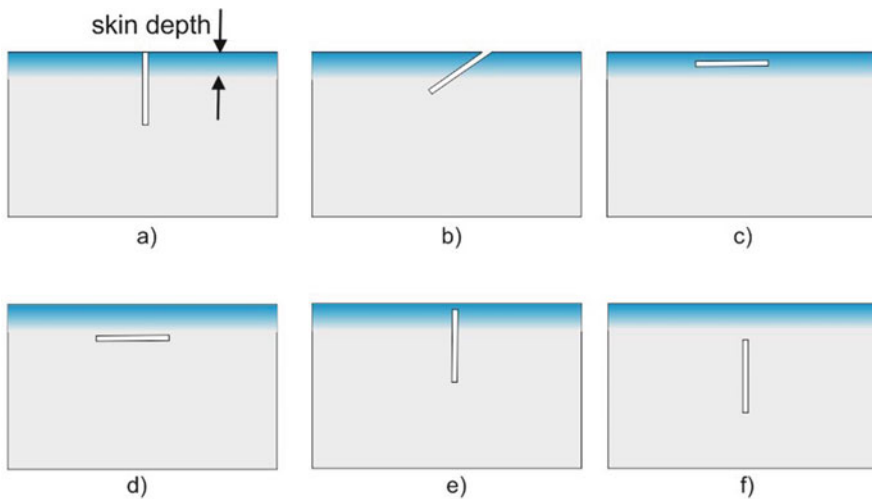

Fig. 5 Some types of cracks to be detected by induction thermography. Types (**a**) to (**e**) are basically detectable, type (**f**) is not directly detectable

The perpendicular crack (a) interacts with the induced current flow and then with lateral heat flows and can therefore be detected. The slanted crack (b) interacts with the current flow, but also with the heat, which is captured in the wedge between crack and surface. Slanted cracks are even better detectable than cracks perpendicular to the surface, which favors detection of forging or rolling laps. Crack type (c) would hardly be detectable by eddy current techniques, but it will produce a thermal contrast, as the heat generated between crack and surface cannot directly flow into the depth. The crack is detected only thermally, comparable to optical surface heating. This is also true for case (d), as long as the crack is located within the thermal diffusion length and its lateral dimension is larger than the coverage. The hidden crack (e) will be detectable as long as the coverage is smaller than half the skin depth (Walle et al. 2012). In the case (f), the crack has neither electromagnetic nor thermal interaction and will therefore not generate a thermal contrast. But case (f) can be converted to case (e), when the skin depth is increased by lowering the induction frequency. An example will be given in the application section.

Another aspect is the orientation of the induced currents with respect to the crack direction. Generally, the thermal contrast will be weaker if the induction current is incident in the crack direction and it will be maximal if it is incident perpendicular to the crack. For ferritic steel, several studies showed that if the angle between crack direction and direction of the induced currents is varied from 90° to 0°, the thermal contrast decreases from 100% down to about 30%, which still allows crack detection with reduced signal/noise ratio (Walle and Netzelmann 2006). Nevertheless, for highest detection sensitivity, it may be necessary to perform two subsequent measurements with orthogonal field orientation or to use an inductor with a rotating induction field.

Detectable Defect Sizes

Validation studies were performed with the aim to determine detection limits of induction thermography. The materials studied were ferritic steel S235, austenitic steel X5CrNi18–10, copper Cu-ETP F25, and aluminum AlNg3. Test bodies from these materials were manufactured including artificial cracks (short notches with a width of 0.3 mm) produced by spark eroding. Perpendicular and slanted cracks of different depths and lengths were investigated. From the measurements, the S/N ratio achieved was determined.

The S/N is usually determined from $C_a/\Delta T_n$, where ΔT_n is the noise level and C_a is the absolute defect contrast

$$C_a = \Delta T_{\mathrm{def}} - \Delta T_s. \tag{8}$$

Here, ΔT_{def} is the temperature change at the defect position and ΔT_s is the temperature change without the defect. The latter can approximately be determined in a sound region close to the crack, which is not yet affected by the crack contrast. In an analog way, an absolute phase contrast of the defect can be determined.

Results for the S/N from artificial cracks in ferritic and austenitic steel obtained from the absolute temperature contrasts are summarized in Fig. 6 (Walle et al. 2009). The results show that the smallest cracks are detectable in ferritic steel and that inclined cracks are detected with more sensitivity than perpendicular cracks. The sensitivity of detection is comparable to that of MT.

For forged ferritic steel, it was shown that for small surface cracks, the signal contrast varies roughly with the product of crack length and crack depth, with saturation occurring towards very long and very deep cracks. Detection of very shallow and small cracks will require short induction pulses and fast camera frame rates.

Determination of the Crack Depth

A major advantage of induction thermography vs. magnetic particle testing (MT) is due to the fact, that induction thermography has the potential to give information on the crack depth. This is hardly possible in MT. If this information were available, in many production processes it could be decided if a component with a detected surface crack is worth to be reworked by grinding a small layer of material. By this, the crack could be removed completely. While the focus in research on induction thermography has been the detection of defects, in the last years there was activity aiming at defect characterization, in particular depth determination of cracks.

• surface cracks perpendicular to the surface			
steel	crack depth [mm]	crack length L [mm]	S/N [dB]
S235	$d \geq 0.15$	$L \geq 7.5$	> 10
	$d \geq 0.25$	$2 \leq L < 7.5$	> 10
X5CrNi18-10	$d \geq 0.3$	$L \geq 5$	6
	$d \geq 0.5$	$2 \leq L < 5$	6
• slanted surface cracks (depth d measured perpendicular to the surface)			
steel	crack depth [mm]	crack length L [mm]	inclination angle α [°]	S/N [dB]
S235	$d \geq 0.08$	$L \geq 7.5$	$20° \leq \alpha \leq 60°$	> 10
	$d \geq 0.15$	$2 \leq L < 7.5$	$20° \leq \alpha \leq 60°$	> 10
X5CrNi18-10	$d \geq 0.20$	$L \geq 5$	$30° \leq \alpha \leq 60°$	6
	$d \geq 0.35$	$2 \leq L < 5$	$30° \leq \alpha \leq 60°$	6
• covered, perpendicular cracks			
steel	cover: z	crack length [mm]	S/N [dB]
S235	$z \leq 0.05$ mm	$L \geq 7.5$ mm	6
X5CrNi18-10	$z \leq 1$ mm	$L \geq 7.5$ mm	6

Fig. 6 Experimentally determined detection limits in two types of steel for different types of cracks

The signal of a crack indication is usually characterized by the relative crack contrast

$$C_r = \frac{\Delta T_{\text{crack}} - \Delta T_s}{\Delta T_s},\tag{9}$$

where ΔT_{crack} is the temperature change at the crack. An analogous procedure is also common when phase images are evaluated.

A detailed analysis on crack depth determination in induction thermography can be found in Oswald-Tranta (2018). Infinitely long cracks were considered. Some results are cited in the following.

With the exception of a special case, there is no analytical formula for the crack contrast as a function of the crack depth d. Numerical simulations that were confirmed by experiments have the following results:

- The relative crack contrast C_r is between -1 and $+1$.
- The crack contrast is determined by δ/μ_T, the ratio of crack depth d to the thermal diffusion length, the relation of the crack depth to the skin depth d/δ and the heating pulse duration t_p.
- For ferritic steel (material group I in Table 1) and cracks with $d >> \delta$, the absolute phase contrast across the crack shows a maximum at the crack position and two minima beside the crack. The depth of the minima increases with crack depth d. There is a saturation effect for deeper cracks, which can be overcome by increasing the pulse length t_p, at the cost of probably missing shallow cracks.
- For nonmagnetic materials (material groups II and III in Table 1) and cracks with $d \approx \delta$, the absolute phase contrast shows a minimum at the crack position. The minimum is deeper with increasing crack depth d. Shorter pulse durations t_p increase the phase contrast.
- The relative amplitude contrast C_r may change its sign with time for larger skin depth. The absolute phase contrast may change its sign with increasing pulse duration t_p for larger skin depth.
- Slanted cracks show asymmetric contrast profiles and need more effort to extract the defect depth from the images.

The Role of the Crack Width

There is a difference between artificial cracks that are machined into a surface and real cracks, which are more irregular in shape and sometimes have local contact points between the crack flanks. In thermography, an open natural crack and most artificial crack represent a line of higher emissivity in the thermography image. This is superimposed onto the contrasts caused by the disturbed current flow. This contrast decreases, when the crack width becomes smaller. On the other hand, the crack contrast can show a chain of local maxima along the crack, if there are several contact points between the crack flanks (Vrana et al. 2008). The induction currents

Fig. 7 Thermographic phase image at an analysis frequency of 2.5 Hz. The images sample size is 40 mm $\times$ 20 mm
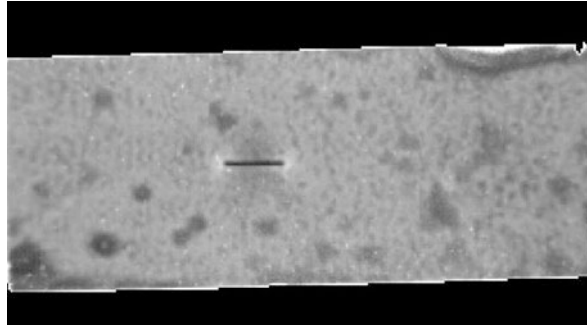
concentrate at these points and generate strong indication in the thermal image. This was also observed for open cracks, which were contaminated by metal chips and dust.

Crack Detection under Nonconducting Coatings

Often surface defects in metals have to be detected under nonconducting coatings. Examples are cracks in turbine blades with ceramic thermal barrier coatings or corrosion spots under paint layers. Defects under coatings can be detected well as long as the coating is thermally thin. Then, the crack is even detected with higher S/N due to the increased surface emissivity (the well-known effect of surface blackening). Even for thermally thick coatings there is a chance for detection, if the coating is partially transparent for the thermal infrared. This is the case for ceramic thermal barrier coatings in the MWIR. But also polymer coatings are often partially transparent in the thermal infrared (Wang et al. 2018). Figure 7 shows the signal of an artificial crack with 5 mm length, 3 mm depth, and 0.5 mm width in ferritic steel obtained by pulse-phase thermography with $t_p = t_c = 0.2$ s. The crack is hidden under a polymer coating of 0.36 mm thickness.

The weak structures in the area around the crack are due to a lack of adhesion of the coating on the steel.

Typical Applications

Steel Components

A study on forged steel parts of very different shapes (Walle and Netzelmann 2006) has shown that typical cracks occurring in such parts can be detected well by induction thermography. There was a first reliability study that indicated a good detection rate and low false alarm rate for induction thermography, whereas MT, as performed under production conditions, often suffered from a high number of false alarms.

In this and other studies, mainly pulsed high-frequency bursts were used, which are probably the best approach, when the available testing time is small. Using periodically modulated high-frequency signals and lock-in processing, crack testing can be achieved at much lower excitation powers of some tens of Watts or less (Riegert et al. 2004). The example shown in Fig. 8 was obtained at about 20 W induction power with a measurement time of 3.5 s. It can be seen that two radially oriented cracks are detected with good contrast in the amplitude and the phase image (Fig. 8c, d). Contrasts on the conical surface (Fig. 8b) due to reflection of external heat sources (in this case lamps in the laboratory) are suppressed by the lock-in calculation.

Another application demonstrates the detection of hardening cracks on a large geartooth (Fig. 9). The crack indication obtained by pulsed induction thermography is shown along with the conventional MT image as obtained under UV light. A concept for an automated manipulator was developed that scans all relevant faces of the test object.
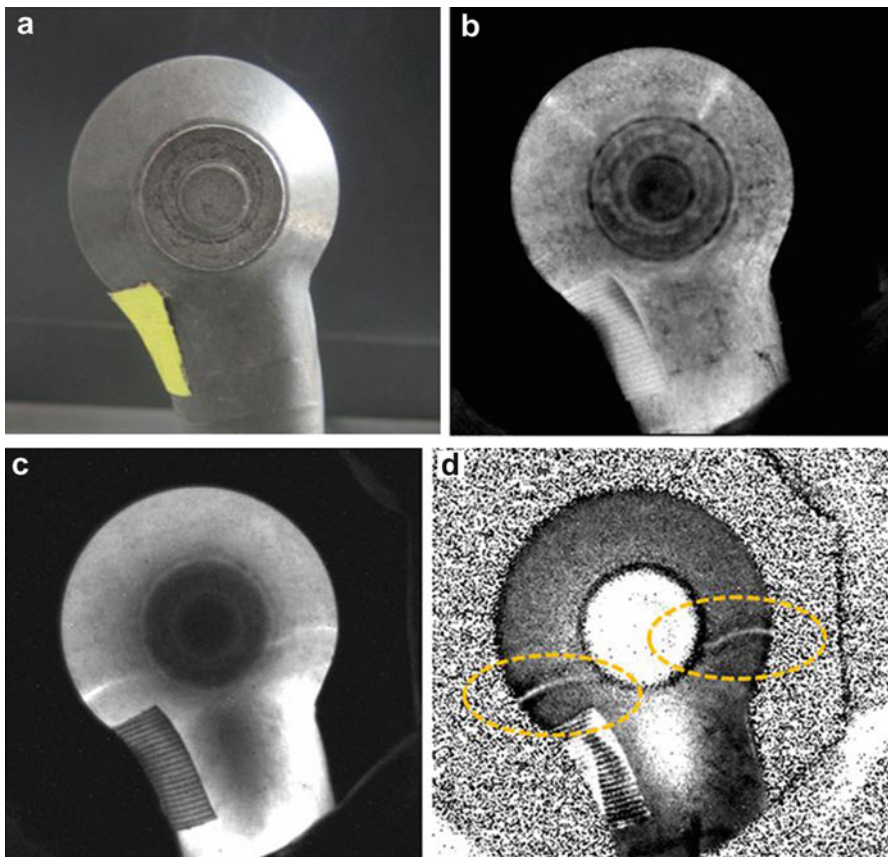

Fig. 8 (**a**) Photo of the forged part. (**b**) Thermographic image before inductive heating, (**c**) Thermographic amplitude image at 4.5 Hz, (**d**) Thermographic phase image at 4.5 Hz. Image size 57 mm × 60 mm. Crack locations are marked

Fig. 9 Hardening crack on a gear-tooth detected by induction thermography (small inset) and by magnetic particle testing (large picture). Image size (inset): 22 mm × 60 mm
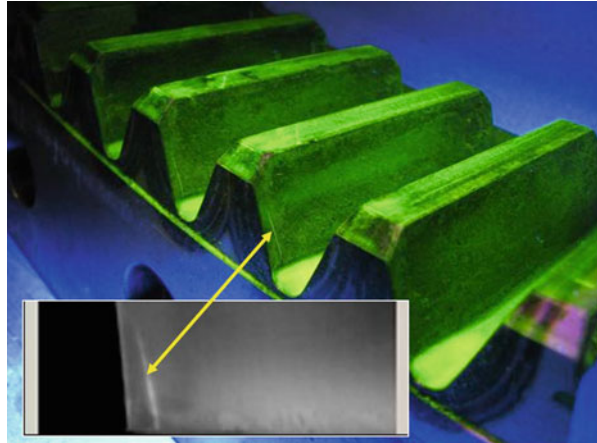
Detection of Hidden Defects in Ferritic Steel

As discussed before, for hidden cracks perpendicular to the surface, the only way to detect the crack by induction thermography is to enlarge the skin depth to at least half of the crack coverage. As a typical skin depth in ferritic steel is about 50 μm, low-frequency power induction generators are required to meet this condition for cracks with coverage of some 100 μm. Figure 10 shows thermographic images of a natural hidden crack with a distance to the surface of 140 μm (as later verified by metallography, Fig. 10c). At 100 kHz induction frequency, there is only a weak contrast (Fig. 10b). If the induction frequency is reduced to 1500 Hz, there is sufficient electromagnetic interaction with the crack and a large crack contrast is obtained. The results were further supported by numerical simulations (Walle et al. 2012). Frequencies down to 300 Hz were used to detect hidden notches. A ratio of coverage to skin depth smaller than 0.5 is required to detect a hidden vertical crack. In the case shown in Fig. 4a, this ratio was 0.34. For the low-frequency experiments, a high-power audio-frequency amplifier was employed.

Testing in Relative Movement and HandHheld Induction Systems

Following the success of the Them-o-Matic (or ELKEM) system (Kremer 1984), several systems with modern infrared cameras and advanced processing were set up. One example is the system DEFECTOVISION® IR by Institut Dr. Foerster GmbH & Co. KG, Germany (Fig. 11). Long round and square steel bars products are inspected for surface defects. Not only single thermographic images but sequences of images are processed. This allows suppression of false indications and an estimation of the defect depth. Bar dimensions of 50 to 220 mm can be tested. The testing speed is up to 1.5 m/s (Koch 2014).
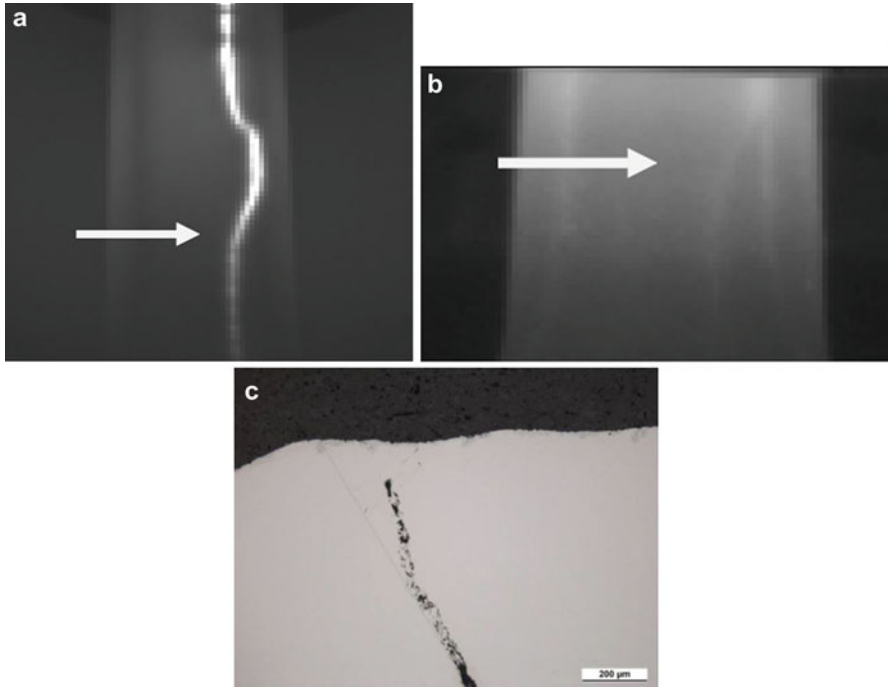
Fig. 10 (**a**) Signal of a natural hidden crack in ferritic steel detected by induction thermography at 1500 Hz excitation frequency. Image size 40 mm × 45 mm. (**b**) The same area imaged by induction thermography at 100 kHz. Image size 13 mm × 30 mm. (**c**) Metallographic cross-section along the arrow
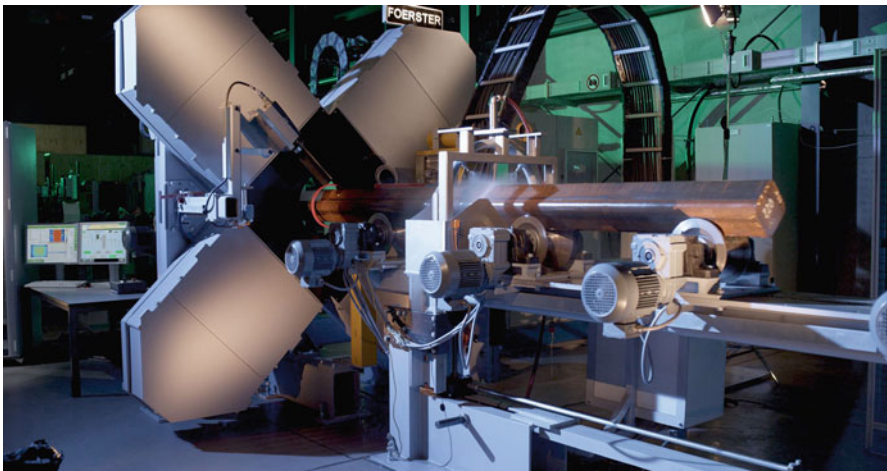

Fig. 11 View of the DEFECTOVISION® IR testing system. (Source: Institut Dr. Foerster GmbH & Co. KG, with permission)

Hand-held induction systems were reported that allow mobile testing. A system developed by Siemens AG CT consists of a hand-held unit with inductor, small IR camera, and display which is connected to a rack with the power electronics (Vrana et al. 2008). Another portable solution is the ITS100 induction thermography system by Qi2/Quest Integrated, LLC. The system consists of a hand-held heating unit and a separate power generator.

Semiconductors

Thermographic techniques have proven to be very useful for characterization of localized defects of different nature in solar cells (Breitenstein et al. 2003). Induction thermography can also be used for testing of solar cells, as silicon is a moderate electrical conductor. Silicon is a good thermal conductor and belongs to material group IV (Table 1). One task is to detect cracks in the silicon in production processes. At usual induction frequencies, the electromagnetic skin depth is of the order of a few cm. Therefore currents are generated in the full volume of a typical cell. As silicon is quite transparent in the thermal infrared, the radiation detected is usually originating from the back-side metallization. Cracks in the brittle material can be long, but they are visually difficult to recognize. Currents that were induced by a coil on the back-side of the cell have to circumvent the cracks and produce a rapidly decaying but strong thermal signal. For the measurement shown in Fig. 12 was obtained in transmission arrangement. The coil was placed behind the sample. A 70 ms long burst pulse at 180 kHz was applied. The image shows a long crack accompanied by thermal contrasts. The thermal pattern of the circular coil is visible in the image.

Carbon Fiber-Reinforced Polymer (CFRP)

Carbon fiber-reinforced polymers (CFRP) are electrically conducting due to their content of carbon fibers. Beside the conduction in fibers and at their contact points, displacement currents are flowing in the dielectric matrix. According to Table 1, the skin depth at typical induction frequencies is of some centimeters. Therefore,
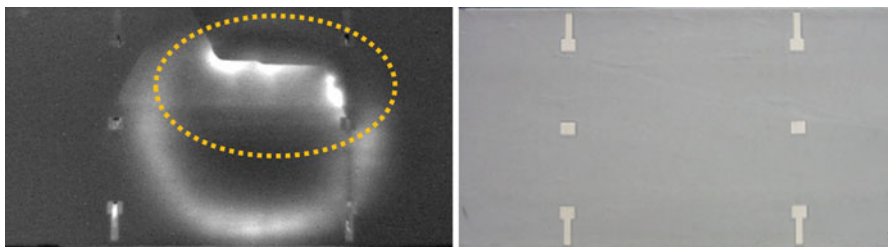

Fig. 12 Left: Thermographic image of a solar cell with crack (marked) Image size 85 mm × 155 mm. Right: Corresponding photo of the back side of the solar cell
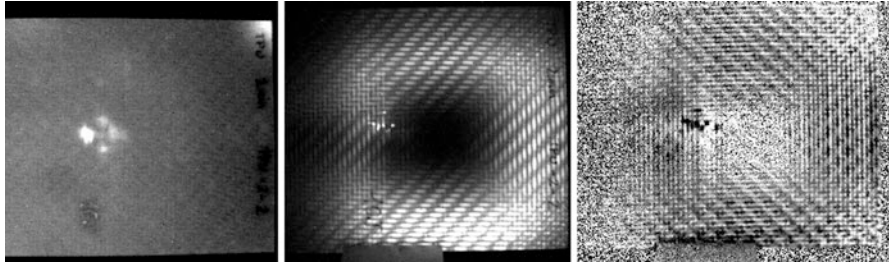
Fig. 13 Left: Detection of an impact damage in CPRP by flash excited thermography. Image size is 100 mm × 100 mm. The same area was imaged by induction thermography with lock-in excitation. Middle: amplitude image. Right: phase image (at 9 Hz modulation frequency)

components are often more of less homogeneously heated. But the current paths in the compound can be very different from that of a metal (Guo et al. 2017), in particular in uni-axial CFRP. Although the heating efficiency can be very good, flash thermography is often better to detect typical impact damage. Figure 13 shows a comparison. The impact damage is revealed clearly in the flash thermographic image. In the corresponding induction thermographic image, the contrast is dominated by the pattern of the carbon fibers in the proximity of the induction coil, which was located behind the CFRP plate. The induction frequency was about 250 kHz. The amplitude and the phase contrast obtained suggest that inductive excitation detects predominantly the fiber damage and less the inner delaminations, which is understandable when considering the largely homogeneous heating over the plate thickness.

In order to reduce the skin depth significantly, experiments were performed at frequencies of 10–30 MHz (Lehtiniemi and Hartikainen 1994) or 52 MHz (Netzelmann et al. 2016b). In the frequency range of some tens of MHz, the skin depth can be reduced to the order of a millimeter.

Railway Component Testing

Rail Surface Defects

Rail surface defects may be caused by rolling contact fatigue of the wheel and rail head.

In rails, crack-like defects (e. g. squats) may occur that are entering the rail head at a small angle. For rail testing, highly developed test cars equipped with ultrasound and eddy current devices have been in operation for many years. In order to check the possibility of induction thermography to find such surface defects in rails, a first preliminary experiment was performed on a German railway test site (Netzelmann et al. 2016a).

After tests in the laboratory and simulation work, a measurement system for induction thermography was adapted for the application in the test car (Fig. 14). An infrared camera pointed at the top surface of the rail and an inductor were mounted
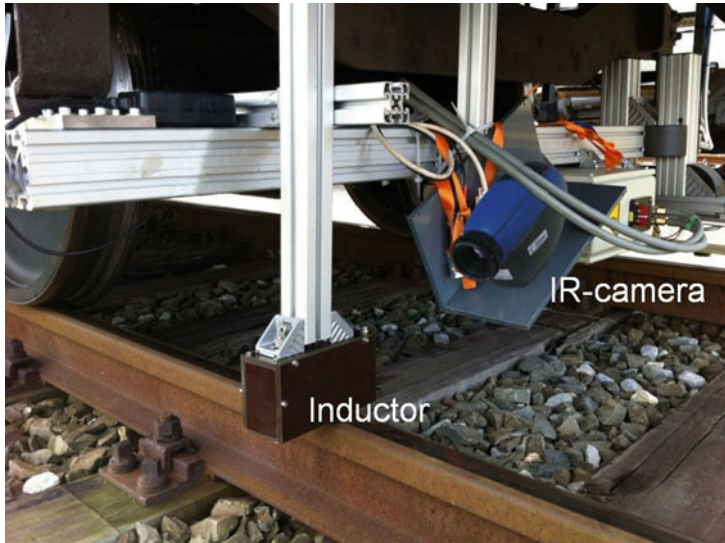
Fig. 14 Thermographic set-up for rail surface defect testing mounted under a test car

under the car close to the rail surface. The induction generator was operated in cw permanent mode and therefore required water cooling. The induction generator and the cooling equipment as well as the data recording were located in the car. The inductor is located inside a box. The camera can detect the defect contrast after it has left the area hidden by the inductor box. The time delay is acceptable due to the relatively high speed of movement.

A thermographic indication of a natural crack-like surface defect taken from the thermography image sequence without further processing is shown in Fig. 15a. It was recorded at a test car speed of 2 km/h. The defect has just left the inductor box, which appears on the right side in Fig. 15a. Measurements were performed at different speed of the test train. The crack contrast decreased with train speed, but could be detected well up to a speed of 15 km/h.

Using properly designed inductors, defects should be not only detectable on the top of the rail, but also in the curved regions between rail top and rail web. Here, other type of sensors would fail due to uncontrollable relative lateral movements between car and rail.

Wheel Surface Defects Detected by a Fully Automated Testing System

The flexibility of camera based solutions and the proven sensitivity of induction thermography to surface defects is also the basis for a demonstrator for thermographic crack detection on railway wheels, which has been set up in Fraunhofer IZFP (Fig. 16) (Ehlen et al. 2016). Wheels are tested directly after production. The infrared camera and the inductor are moved by a robot. The wheel is fixed on a rotation stage where it can be scanned in concentric tracks over the hub, disk, and tread of the wheel. The robot keeps the required distance and direction of the arrangement of
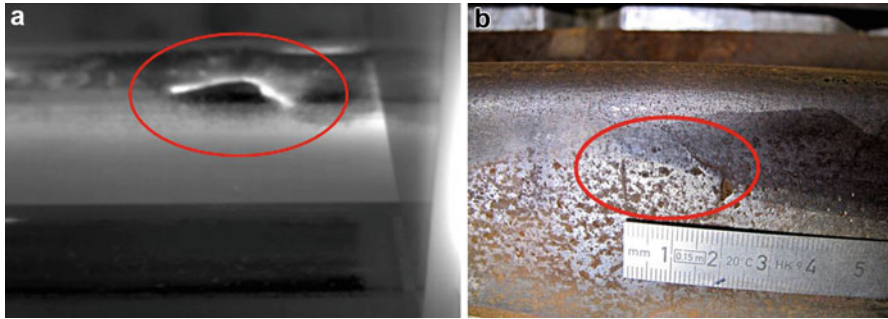
Fig. 15 (**a**) Thermographic image of a rail surface defect obtained at a speed of 2 km/h. Image size is about 70 mm × 93 mm. (**b**) Photo of the defect area taken in the laboratory

Fig. 16 Demonstrator set-up for surface defect testing on railway wheels by induction thermography using a robot

inductor and camera. Thermographic image acquisition and image processing including defect recognition are performed in parallel. Results are presented in polar plots with markings of the detected defects.

Wheels with artificial test defects and with natural defects were tested. The present detection limits are cracks of 0.1 mm depth and 3 mm length. The sensitivity of the system can compete with that of magnetic particle testing. The total testing time for a wheel is below 10 min.

Comparison of Induction Thermography and Magnetic Particle Testing

Standard NDT techniques for testing components for surface defects are magnetic particle testing (MT) and liquid penetrant testing (PT). Ferritic steel parts are often manufactured in mass production for the automotive industry. Therefore, in this industrial branch, there is big interest for fast, fully automated NDT solutions.

For MT, the testing agent is first sprayed on the component. The agent consists of a suspension of small ferromagnetic particles. By an external magnetic field or by a magnetic field generated by an external current, a magnetic flux with a strong component parallel to the surface is generated. At cracks, the magnetic flux is diverted into the region outside the component surface. The magnetic particles aggregate at the position of the maximum gradient of the magnetic field, which is the opening of the crack. Often, a fluorescent testing agent is used, where a dye is coupled to the magnetic particles. The dye emits light under excitation by a UV lamp and thereby marks the crack visible for the testing person. After the evaluation of the crack indication, the magnetic field is switched off. Then the testing agent usually has to be flushed off the surface. Disadvantages of this technique are:

- The evaluation of the test results depends on the inspector and his or her concentrated attention during the testing process.
- The differentiation between false indications and real defects is very difficult and requires an experienced inspector.
- Additional effort arises due to the necessity to remove the magnetic particle testing fluid. Sometimes demagnetization of the component is required.
- The chemicals involved are partly toxic and costly to dispose. UV radiation can be harmful to health.
- There are no digital raw data available for analysis after the surface crack detection process.

In comparison to MT, the main advantages of induction thermography are:

- The technique is working without direct contact, extensive and fast.
- Induction thermography allows detection of shallow subsurface cracks.
- By analysis of the phase signal profiles over the crack, an estimation of the crack depth is possible.
- It is not necessary to treat the surface with a couplant or particle suspension. Disposal costs and environmental hazards are avoided.
- It is usually not necessary to demagnetize a test object after testing.
- Induction thermography allows one to test the components in a fully automated objective way according to defined criteria.

Standardization

There is considerable interest in industry on induction thermography. Up to now, however, introduction of this technique was impeded by missing standardization. A work around complex individual qualification by expertise or validation is possible. As this process is too costly and tedious in particular for small and medium enterprises, general standardization of induction thermography is desired.

In the last years, old standards on thermography were updated according to the progress of the state-of-the art. There is now a new European standard EN 16714 Nondestructive testing – Thermographic testing, containing the topics "General principles" (part 1), "Equipment" (part 2) and "Terms and definitions" (part 3). There will be a completely new European standard on active thermography based on DIN 54192. It will be followed by a European basic standard for induction thermography based on the German standard DIN 54183, which has been released at the end of 2017.

Summary and Outlook

Induction thermography can be applied to a wide range of materials that exhibit at least some electrical conductivity. Its ability to detect both surface cracks and hidden cracks close to the surface is very attractive, in particular for inspection of ferritic steel. The advantage of induction thermography compared to magnetic particle testing lies in the noncontact operation avoiding particle solutions and chemicals, as well as the ability to offer fully automated testing and well-documented results.

Cracks in ferritic steel can usually be detected with good signal/noise ratio. Progress has been obtained in determining the defect depth from the thermographic data.

An application with difficulties is crack detection on highly reflecting aluminum alloys and other materials with highly reflecting surfaces and low emissivity. Simulations and experimental evidence show that the contrast obtained from a crack in aluminum may be one to two orders of magnitude smaller than that of magnetic steel.

A central requirement for an alternative testing technique, however, is at least equal detection sensitivity and reliability as the existing standard. Although present results show that relevant cracks can be detected reliably, there is a demand for research on long-term stability and reliability in mass production applications.

More pilot applications and upcoming application standards will increase the acceptance of the technique.

References

Balaji L, Balasubramanian K, Krishnamurty C (2013) Induction thermography for non-destructive evaluation of adhesive bonds. In: Review of progress in quantitative nondestructive evaluation, vol 39, AIP conference proceedings 1511, pp 579–586

Bamberg J, Erbeck G, Zenzinger G (1999) Eddy-Therm: Ein Verfahren zur bildgebenden Prüfung metallischer Bauteile. ZfP-Zeitung 68:60–62

Bowler N (2006) Frequency-dependence of relative permeability in steel. Rev of Quant NDE 25:1269–1276

Breitenstein O, Rakotoniaina J, Al Rifai M (2003) Quantitative evaluation of shunts in solar cells by lock-in thermography. Prog Photovolt Res Appl 11:515–526

Carslaw H, Jaeger J (1959) Conduction of heat in solids. Claredon Press, Oxford, p 80

Ehlen A, Netzelmann U, Lugin S, Finckbohner M, Valeske B, Bessert S (2016) Automated NDT of railway wheels using induction thermography. In: Proceedings of the 55th annual conference of the British Institute of non-destructive testing, Nottingham

Guo J, Gao X, Toma E, Netzelmann U (2017) Anisotropy in carbon fiber reinforced polymer (CFRP) and its effect on induction thermography. Nondestr Test Evaluat Int 91:1–8

He Y, Tian G, Pan M, Chen D (2014) Impact evaluation in carbon fiber reinforced plastic (CFRP) laminates using eddy current thermography. Compos Struct 109:1–7

Heath D, Winfree W (1990) Quantitative thermal diffusivity imaging of disbonds in thermal protective coatings using inductive heating. In: Thompson DO, Chimenti DE (eds) Review of progress in quantitative nondestructive evaluation, vol 9. Plenum Press, New York, pp 577–584

Jäckel P, Netzelmann U (2013) The influence of external magnetic fields on crack contrast in magnetic steel detected by induction thermography. QIRT J 10:237–247

Koch S (2014) Non-destructive testing of bars by inductive heat-flux thermography. Millenium Steel India, pp 140–142

Kremer K J (1984) Das THERM-O-MATIC-Verfahren – Ein neuartiges Verfahren für die Online-Prüfung von Stahlerzeugnissen auf Oberflächenfehler. In: Proceedings of the 3rd European conference in nondestructive testing, Florence, 15–18 October 1984, pp 171–186

Lehtiniemi R, Hartikainen J (1994) An application of induction heating for fast thermal nonde-structive evaluation. Rev Sci Instrum 65:2099–2101

Liang T, Ren W, Tian GY, Elradi M, Gao Y (2016) Low energy impact damage detection in CFRP using eddy current pulsed thermography. Compos Struct 143:352–361

Netzelmann U (2006) German Patent DE102006050025B3

Netzelmann U, Walle G (2008) Induction thermography as a tool for reliable detection of surface defects in forged components. In: Proceedings of the 17th World conference on nondestructive testing, 25–28 Oct 2008, Shanghai, China

Netzelmann U, Walle G, Ehlen A, Lugin S, Finckbohner M, Bessert S (2016a) NDT of railway components using induction thermography. In: AIP conference proceedings 1706, 150001

Netzelmann U, Walle G, Lugin S, Ehlen A, Bessert S, Valeske B (2016b) Induction thermography: principle, applications and first steps towards standardization. QIRT J 13:170–181

Oswald-Tranta B (2004) Thermoinductive investigations of magnetic materials for surface cracks. QIRT J 1:33–46

Oswald-Tranta B (2018) Induction thermography for surface crack detection and depth determina-tion. Appl Sci 8:257

Riegert G, Zweschper T, Busse G (2004) Lockin thermography with eddy current excitation. QIRT J 1:21–32

Tang B, Hou D, Hong T, Ye S (2018) Influence of the external magnetic field on crack detection in pulsed eddy current thermography. Insight 60:240–246

Tsopelas N, Siakavellas N (2011) Experimental evaluation of electromagnetic-thermal non-destruc-tive inspection by eddy current thermography in square aluminum plates. NDT & E Int 44:609–620

Vrana J, Goldammer M, Baumann J, Rothenfusser M, Arnold W (2008) Mechanisms and models for crack detection with induction thermography. In: Review of progress in quantitative nonde-structive evaluation, vol 27, AIP conference proceedings 975, pp 475–482

Walle G, Netzelmann U (2006) Thermographic crack detection in ferritic steel components using inductive heating. In: Proceedings of the 9th ECNDT Berlin, 25–29 Sept 2006, DGZfP Berichtsband BB 103

Walle G, Valeske B, Netzelmann U (2009) Eine thermische Prüftechnik zur Oberflächenrissprüfung leitfähiger Materialien. Materialprüfung (9):593–602

Walle G, Netzelmann U, Stumm C, Valeske B (2012) Low frequency induction thermography for the characterization of hidden cracks in ferromagnetic steel components. In: Proceedings of the 11th international conference on quantitative infrared thermography (QIRT), 11–14 June 2012, Naples, Italy, paper 218

Wang Y, Gao X, Netzelmann U (2018) Detection of surface cracks in metals under coatings by induction thermography. In: Proceedings of the 14th quantitative infrared thermography conference, Berlin 25–29 June 2018, DGZfP BB 167

Wilson J, Tian G, Abidin I, Yang S, Almond D (2010) Pulsed eddy current thermography: system development and evaluation. Insight Non-Destr Test Cond Monit 52:87–90

Zenzinger G, Bamberg J, Satzger W, Carl V (2007) Thermographic crack detection by eddy current excitation. Nondestruct Test Evaluat Int 22:101–111